Aeration-driven regulation of heterotrophic ammonia assimilation under high salinity Carbon-nitrogen conversion and microbial community

Zhao, Chuanfu; Zhang, Wenhao; Guo, Yiting; Han, Fei; Zhang, Mengru; Li, Yuke; Zhou, Weizhi

DOI
10.1016/j.jece.2025.117911

Publication date
2025

Document Version
Final published version

Published in
Journal of Environmental Chemical Engineering

Journal of Environmental Chemical Engineering 13 (2025) 117911

Contents lists available at ScienceDirect

Journal of Environmental Chemical Engineering

journal homepage: www.elsevier.com/locate/jece

Aeration-driven regulation of heterotrophic ammonia assimilation under high salinity: Carbon-nitrogen conversion and microbial community

Chuanfu Zhao [a,b], Wenhao Zhang [a,b], Yiting Guo [a,b], Fei Han [a,b], Mengru Zhang [a,b], Yuke Li [c], Weizhi Zhou [a,b,*]

[a] School of Civil Engineering, Shandong University, Jinan, Shandong, PR China
[b] Laboratory of water-sediment regulation and eco-decontamination, Jinan, Shandong, PR China
[c] Department of Water Management, Faculty of Civil Engineering and Geosciences, Delft University of Technology, Stevinweg 1, Delft 2628 CN, the Netherlands

ARTICLE INFO

Keywords:
Heterotrophic ammonia assimilation
Oxygen load
Microbial network
Salinity

ABSTRACT

Oxygen is essential for heterotrophic ammonia assimilation (HAA), driving the microbial degradation of organic compounds and ammonia assimilation in aerobic wastewater treatment. However, the mechanisms underlying carbon-nitrogen transformation and microbial community assembly by heterotrophs under aerobic conditions remained elusive. This study investigated the impact of aeration rates (0.1, 0.5, 1, and 3 L/min·L) on the pollutant removal and microbial dynamics of HAA bioreactors over a 120-day operation period to improve the performance of the system by regulating the microbial oxygen affinity. The NH_4^+-N and COD removal efficiencies of the highest aeration rate (3 L/min·L) were as high as 94.8 % and 96.8 %. Batch tests on nitrogen balance verified that nitrogen removal was attributed to assimilation rather than nitrification. The kinetic and mass balances analysis highlighted enhanced microbial activity and substrate utilization at increased aeration rates. *Halomonas*, emerged as dominant taxa, correlating with improved ammonia assimilation under higher aeration rates. Increased aeration enhanced the microbial robustness and reduced the modularity of microbial interactions, and stochastic processes emerged as the primary drivers of community assembly. The aeration rates of 1–3 L/min·L were considered as the parameter range of optimal pollutant removal, and the aeration rate parameter close to 1 L/min·L was considered as the optimal efficiency combined with the cost. This study provides valuable insights for optimizing biotechnological applications and engineering microbial systems for enhanced environmental performance.

1. Introduction

Efficient carbon and nitrogen conversion remains a central challenge in wastewater treatment, especially in mitigating nitrogen pollution, which causes eutrophication and ecological degradation. Traditional processes like nitrification and denitrification are not only energy-intensive but also result in substantial losses of carbon and nitrogen resources, alongside greenhouse gas emissions. These challenges are further amplified in the context of high-salinity wastewater, which is increasingly common in industrial effluents and poses additional stress to conventional microbial systems [1,2]. High-salinity wastewater is rich in nitrogen and phosphorus, but saline stress often inhibits conventional biotreatment efficiency. The complete nitrification is hardly achieved when the salinity is higher than 20 g NaCl/L, since nitrite accumulation occurred [4]. The IC_{50} of NaCl was calculated as 42.1 g/L in microbial community of anammox (Zhang et al., 2022d). However, salinity strongly inhibits anammox activity by reducing the specific growth rates of most species, with only *Ca. Scalindua* showing high salinity tolerance above 2 % [5].

Biotreatment systems utilizing halophilic or marine-derived microorganisms have shown promise under saline conditions. Halophilic heterotrophic ammonia assimilation (HAA) offers a promising solution, leveraging the metabolic activity of marine-derived aerobic heterotrophic microorganisms to directly convert ammonia into organic nitrogen under higher salt, which not only achieves nutrient recovery from wastewater but also avoids the production of harmful intermediate products such as nitrite (NO_2^-), nitrate (NO_3^-), and nitrous oxide (N_2O) that are commonly generated during ammonia oxidation. Marine-derived HAA exhibits strong adaptability to salinity due to the inherent halotolerance of marine microbial consortia. Unlike

* Corresponding author at: School of Civil Engineering, Shandong University, Jinan, Shandong, PR China.
E-mail address: wzzhou@sdu.edu.cn (W. Zhou).

https://doi.org/10.1016/j.jece.2025.117911
Received 3 May 2025; Received in revised form 10 June 2025; Accepted 4 July 2025
Available online 5 July 2025

autotrophic bacteria, these heterotrophs maintain metabolic activity and nitrogen assimilation efficiency under high-salinity stress, enabling stable nitrogen recovery in hypersaline environments. HAA offers practical advantages such as a simplified process, smaller footprint, and salinity tolerance, making it suitable for real-world applications. Although it requires more oxygen and carbon input, HAA ensures stable nitrogen recovery by addressing oxygen and carbon imbalances in the overall treatment process. As for the high value-added sludge products generated by HAA, rich in organic matter, residual nutrients (such as nitrogen and phosphorus), and salt-tolerant microbial populations, saline sludge holds promise for improving the structure and fertility of degraded saline-alkali soils. When saline sludge can be subjected to washing, composting, or dilution before land application to mitigate the risk of secondary soil salinization, it can enhance soil microbial activity, promote plant growth, and reduce the salinity stress on crops by improving ion balance and organic carbon content. Additionally, it is most suitable for use in salt-affected or marginal soils where salt-tolerant microbial consortia may improve soil fertility and structure without further aggravating salinity stress.

Dissolved oxygen serves as an essential substrate for aerobic microorganisms. The complete nitrification requires a DO of more than 5 mg/L [9], while partial nitrification typically occurs with a DO content of 0.3–1.5 mg/L [10]. Denitrification maximizes nitrogen removal at 0.5 mg/L [11], while the aerobic granular sludge process requires a DO supply of more than 2 mg/L to achieve satisfactory operating performance [12]. In ammonia oxidation, oxygen serves as the electron acceptor, enabling the conversion of ammonia into nitrite and nitrate by specific microbes (AOB and NOB), and the process is highly sensitive to oxygen levels [13]. By contrast, oxygen during ammonia assimilation not only provides the energy required for metabolism but also influences microbial growth and metabolic pathways, promoting the direct incorporation of ammonia nitrogen into cellular biomass [8]. Oxygen plays different roles in ammonia oxidation and ammonia assimilation reactions, and leads to a more profound impact on the assimilation process.

Efficient and stable HAA operation requires optimizing energy-related parameters, with aeration rate being the key factor controlling dissolved oxygen levels [14]. DO critically affects oxygen transfer, sludge fluidity, and the assimilation efficiency of heterotrophic microbes. Low DO impairs ammonia removal, while excess DO causes shear damage to biomass flocs [13]. Microbial responses to DO are regulated at the genetic level, influencing key metabolic enzymes. Balancing DO is thus essential for optimizing reactor performance and energy use [15], and is key to understanding carbon-nitrogen conversion in aerobic heterotrophic systems.

This study aimed to (1) investigate the different increased aeration rates on the efficiency of heterotrophic ammonia assimilation in wastewater treatment; (2) systematically explore the effects of DO levels on pollutant removal, microbial dynamics and mass balance; (3) reveal the influence of aeration rate gradient on microbial community interaction and assembly.

2. Materials and methods

2.1. Bioreactor operation

Four 1 L cylindrical sequential batch reactors (SBRs) were established with aeration rates of 0.1, 0.5, 1 and 3 L/min·L, respectively, named R1, R2, R3 and R4. The volume exchange rate is 50 %. Four representative values of aeration rate were selected for reference to published studies [16–18]. Each cycle time is 12 h, including 5 min of inlet, 690 min of aeration, 20 min of sedimentation, and 5 min of outlet. The HAA sludge was inoculated in the pilot-scale reactor using synthetic wastewater with a salt content of 3 % as raw material and Marine sediment at the station of A4 (123°2′848″ E, 36°0′614″ N) of the Yellow Sea as the source. The mixed liquid suspended solid (MLSS) of the inoculated sludge was 10 g/L respectively, and the slurry discharge every 10 days kept the MLSS at 10 g/L. The composition of synthetic wastewater simulated seawater blackwater referred to toilet flushing sewage reported by van Voorthuizen [19] (mg/L): COD (as NaAc) 2000, NH_4^+-N (as NH_4Cl) 100, P (as K_2HPO_4) 20, NaCl 30000.

The design and operation of the Batch tests I and II were established from the perspectives of pollutant degradation, oxygen affinity and nutrient element destination at different aeration rates in Text S1. The method of the control test between inactivated sludge and EPS can be found in Text S1. The contents of DO, COD, and N concentrations in each batch tests were determined, and the oxygen half-saturation constant of the four bioreactors were calculated according to the Monod equation (Text S2).

2.2. Analytical methods

The concentrations of COD, TN, NH_4^+-N, NO_2^--N, and NO_3^--N were measured following standard APHA method [20]. Soluble microbial products (SMP) were extracted by centrifuging a sludge -water mixture at 4000 rpm and filtering it through a 0.45 μm membrane [13]. Parameters for three-dimensional fluorescence spectroscopy (3D-EEM) analysis included an emission wavelength (Em) range of 200–450 nm and an excitation wavelength (Ex) range of 280–550 nm, with parallel factor analysis (PARAFAC) [8]. FRI analysis refers to previous literature [21]. Extracellular polymeric substances (EPS) were extracted from sludge samples using an improved thermal method [1]: sludge was centrifuged at 4000 g for 5 min, resuspended in 0.05 % NaCl, diluted to 50 mL, heated at 50°C for 60 min, then centrifuged at 4000 g for 15 min; the supernatant was collected as EPS extract. Protein (PN) and polysaccharide (PS) contents were determined using the anthrone-sulfuric acid and modified Lowry methods, respectively [22]. Methods for determining nitrogen footprints and specific energy demands are detailed in Text S3. Methods for the electrochemical characterizations of EPS, including cyclic voltammetry (CV), and electrochemical impedance analysis (EIS) are detailed in Text S4. The method of 15N-incubation experiments is detailed in Text S5. Elemental analysis was conducted using the elemental analyzer (Thermo Fisher Scientific Flash 2000). Glutamate dehydrogenase (GDH), glutamine synthetase (GS), glutamine synthase (GOGAT), total amino acids (TAA), glutamine (Gln), glutamate (Glu), adenosine triphosphate (ATP) and nicotinamide adenine dinucleotide phosphate (NADPH) in sludge were quantified using corresponding assay kits (Solarbio, Beijing, China) [23].

2.3. Microbial community analysis

Sludge samples were collected for high-throughput sequencing analysis using 515 F and 806 R primers. Specifically, Z1 represents the inoculated sludge at Day 0. Samples Z2–Z4 were taken from bioreactor R1 on Days 40, 80, and 120, respectively. Z5–Z7 were collected from R2, Z8–Z10 from R3, and Z11–Z13 from R4 at the same respective time points. Bacterial genomic DNA was extracted from the sludge samples using the PowerSoil DNA Separation Kit (MoBio Laboratories, Carlsbad, CA, USA). Sequencing data (raw data) are accessible in the National Center for Biotechnology Information (NCBI) database under accession number PRJNA1153392. PICRUSt2 was employed to analyze differences in nitrogen assimilation-related genes in HAA systems at various aeration rates [24]. Microbial networks were constructed using the "psych" and "igraph" packages in R (ver. 4.0.0) for matrix building, with Gephi (ver. 0.9.2) used for visualization and topological analysis. Network robustness, including metrics such as average degree and natural connectivity, was assessed using "igraph" and "ggplot2" in R (ver. 4.0.0). The steps for neutral community and null model calculations are detailed in prior studies [8]. Partial least squares pathway modeling (PLS-PM) was applied to explore relationships among key factors in assimilation metabolism. Niche breadth, Similarity percentage (SIMPER), Procrustes analysis, and Mantel analysis was conducted using

the "ggplot2", "vegan" and "ggcor" packages in R (ver. 4.0.0).

3. Results and discussion

3.1. Long-term performance of bioreactors with different aeration rates

In long-term pollutant degradation performance (Fig. 1A-B and Figure S1), the R1 bioreactor at aeration rate of 0.1 L/min·L showed more fluctuating NH_4^+-N removal performance with an average removal efficiency of 28.0 ± 6.8 %. The suitable nitrogen assimilation environment could not be maintained due to the low oxygen load and solid-liquid fluidity. By contrast, the R2 bioreactor (0.5 L/min·L) began to show more stable operating conditions and a slightly higher NH_4^+-N removal efficiency of 44.4 ± 3.2 %. In R3 and R4 bioreactors (1 and 3 L/min·L), the removal efficiencies of NH_4^+-N were significantly higher, which were 81.3 ± 3.8 % and 94.8 ± 2.2 %, respectively. These improvements could be attributed not only to higher oxygen availability but also to increased biomass. There was little accumulation of NO_2-N and NO_3-N (Figure S1). In comparison to NH_4^+-N removal, the COD removal effects of bioreactors was more satisfactory. The COD removal efficiencies of the R1, R2, R3, R4 bioreactors were 65.4 ± 14.2 %, 75.4 ± 9.6 %, 91.3 ± 4.9 % and 96.8 ± 3.5 %, respectively. The average sludge yields of R1, R2, R3, R4 bioreactors were 0.58, 0.88, 1.59 and 1.84 g MLSS/d·L (Figure S2). The correlation between NH_4^+-N removal content and sludge concentration increase content (R1: $r = 0.973$, $p < 0.001$;) R2: $r = 0.966$, $p < 0.001$; R3: $r = 0.964$, $p < 0.001$; R4: $r = 0.969$, $p < 0.001$) confirmed that the ammonia assimilation reaction with biomass increase was the main way of ammonia removal, consistent with previous research [8].

Notably, the correlation between COD and MLSS revealed that the process of organic oxidation and biomass conversion under low oxygen load is not completely consistent. Limited oxygen was used by heterotrophic microorganisms mainly for respiratory metabolism and not exclusively for nitrogen assimilation-related biomass accumulation. Insufficient DO suppresses the generation of ATP and redox equivalents required for biosynthesis and ammonia assimilation. Although low aeration reduces energy input, it limits microbial metabolism and enzyme expression (e.g., GDH, GS), leading to unstable nitrogen removal [14]. From the perspective of microbial ecology, the halophilic heterotrophs used in the HAA system with prominent ammonia assimilation function are usually aerobic or facultative anaerobic, but lack strong adaptability to continuous hypoxic conditions. While oxygen input should be minimized for efficiency, excessively low aeration compromises both biological activity and system stability in the long term.

3.2. Batch tests performance under different aeration rates

3.2.1. Batch tests I for pollutant degradation analysis

Batch tests I of nitrogen balance with (Fig. 1 C-F) and without ATU (Figure S3) are set up to monitor variations of pollutant concentrations to determine degradation pathways. In the batch test I of R1 bioreactor, the DO was dropped rapidly from an initial 1.18 O_2 mg/L to an average of 0.06 O_2 mg/L. In contrast, DO in R2 bioreactor stabilized at 1.24 O_2

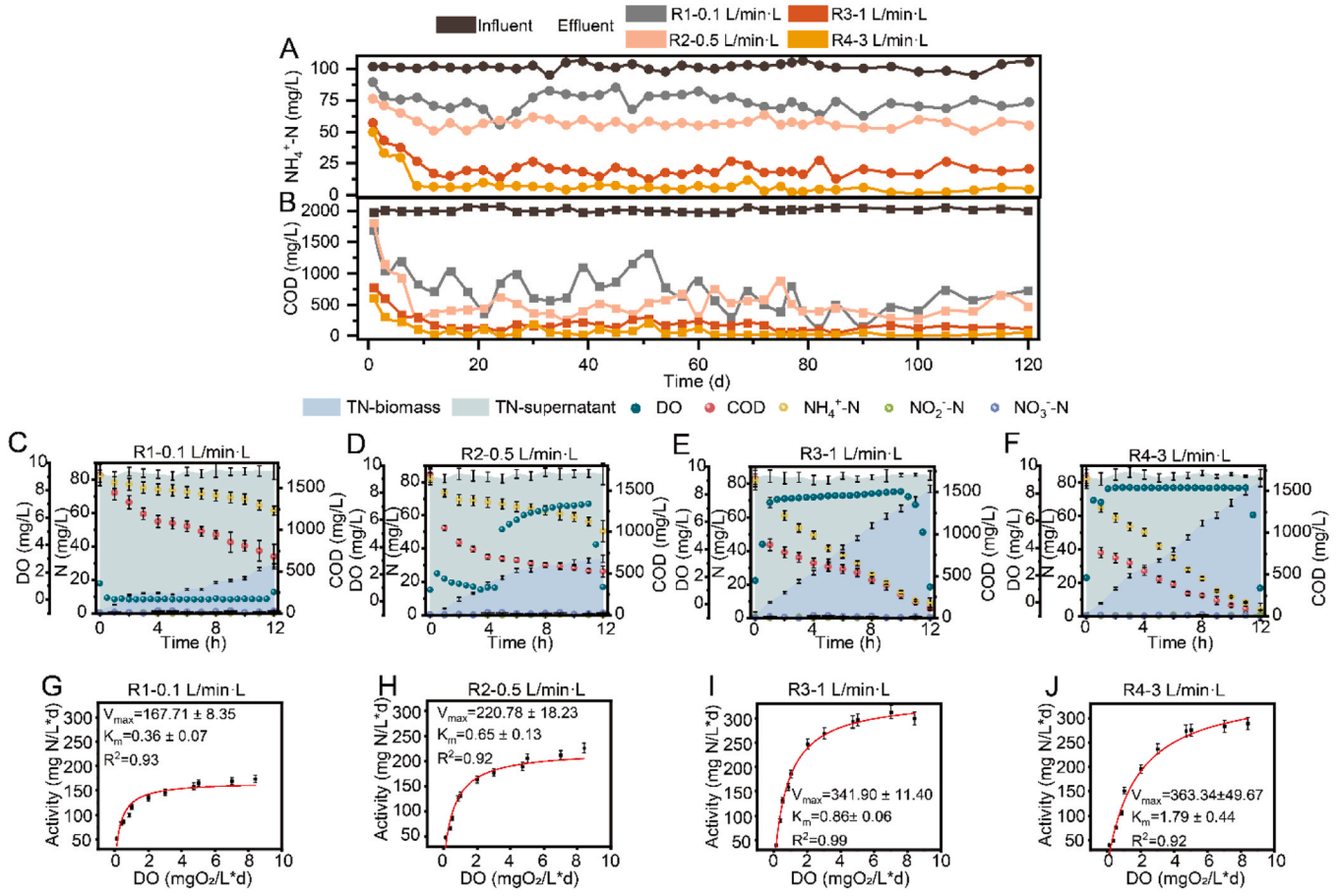

Fig. 1. Treatment performance of heterotrophic ammonia assimilation reaction under different aeration rates: the influent and effluent of (A) NH_4^+-N and (B) COD concentrations. Mechanism analysis of nitrogen assimilation: Batch tests with 30 mg/L ATU addition with aeration rates of (C) 0.1 L/min·L, (D) 0.5 L/min·L, (E) 1 L/min·L and (F) 3 L/min·L. Kinetic analysis of ammonia assimilation capacity of bioreactors with long-term supply aeration rates of (G) 0.1 L/min·L, (H) 0.5 L/min·L, (I) 1 L/min·L, (J) 3 L/min·L.

mg/L at 0–4.5 h, and DO gradually was increased to 7.18 O_2 mg/L with the accumulation of oxygen to the end. The DO changed in the R3 and R4 bioreactors were consistent, reaching a high level of DO state of 7.85 O_2 mg/L and 8.35 O_2 mg/L on average, respectively. The degradation performance of carbon and nitrogen pollutants in long-term operation and typical cycle was consistent. The nitrogen adsorption of biomass and EPS was found to be negligible (<5 % of total TN input) under the tested conditions (Figure S3). The NH_4^+-N removal efficiency showed no significant difference between treatments with and without ATU ($p > 0.05$), and no notable accumulation of other inorganic nitrogen compounds was observed. A linear relationship was identified between the reduction in TN-supernatant and the increase in TN-biomass across the four bioreactors. The absence of significant nitrogen loss suggested nitrogen removal by assimilation rather than by the dissimilation pathway. The degradation kinetics analysis based on nitrogen balance showed that N and COD removal and the generation of biomass were consistent with the pseudo-first-order kinetic model (Figure S4). The apparent rate constant (*kobs*) associated with the increase of aeration rate was smaller, and the small difference between the three *kobs* of the three substances suggested consistency in the carbon nitrogen conversion process. The microbial cell abundance of ^{15}N increased in the four bioreactors in the ^{15}N isotope labeling test, while $^{15}N_2$ and $^{15}N_2O$ were not detected (Table S1).

3.2.2. *Batch tests II for oxygen affinity kinetic analysis*

The oxygen half-saturation constant in the Monod equation based on

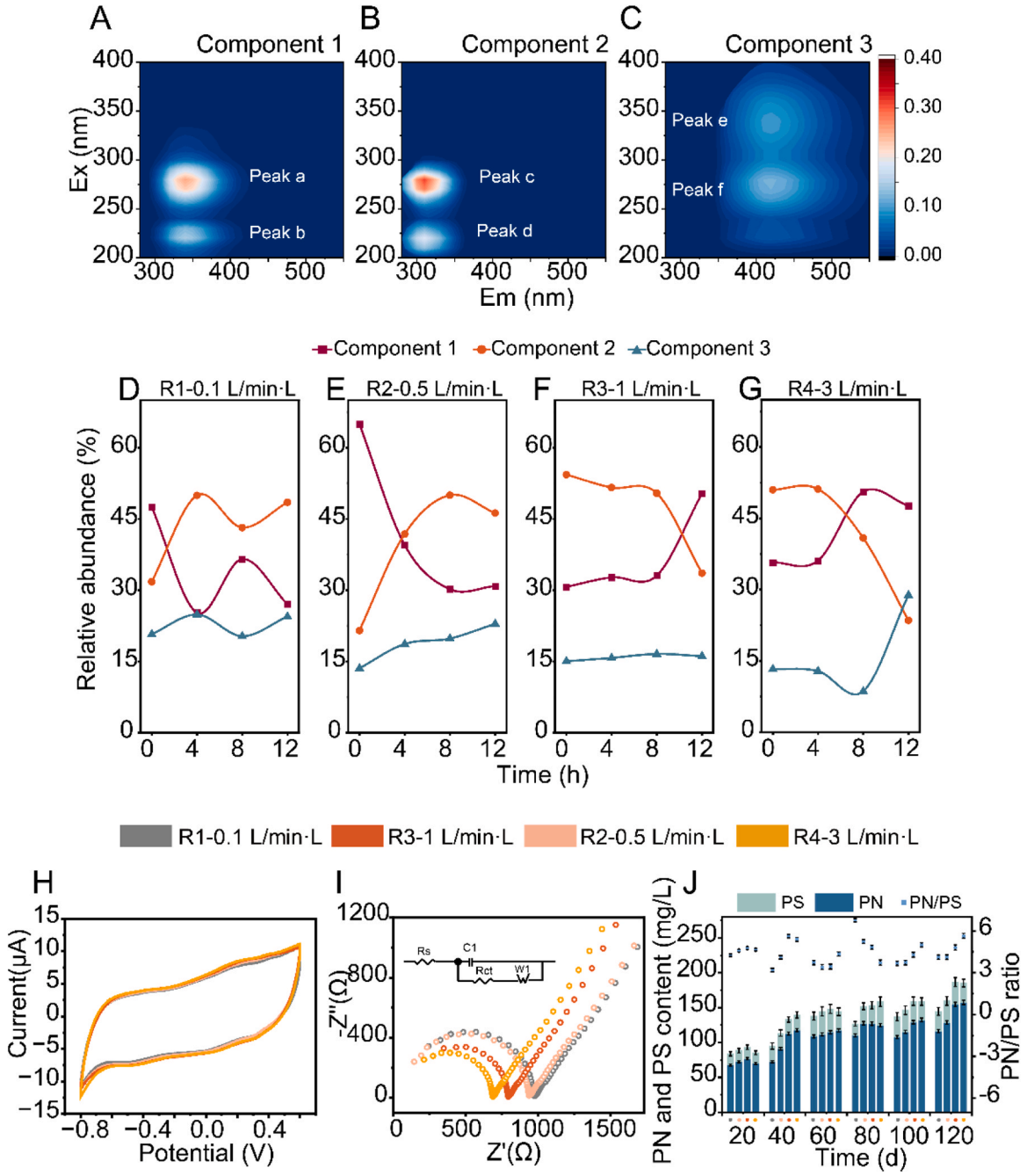

Fig. 2. Three-dimensional fluorescence spectrum analysis of typical cycle samples under different aeration rates: (A) component 1, (B) component 2, (C) component 3, and the Fmax in bioreactors with aeration rates of (D) 0.1 L/min·L, (E) 0.5 L/min·L, (F) 1 L/min·L and (G) 3 L/min·L. Characteristics of extracellular polymeric substrate: (H) CV curves, (I) EIS test and (K) Polysaccharide, protein content and protein-polysaccharide ratio.

cell growth kinetics represented the affinity of microorganisms for oxygen and is crucial for optimizing microbial growth and aeration efficiency in wastewater treatment systems [25]. Batch tests II of different dissolved oxygen states (Figure S5) were established to perform kinetic analysis. In the kinetic analysis (Fig. 1 G-J), the R1-R4 bioreactors underwent complete reaction processed at four aeration rates respectively. The K_m were 0.47 ± 0.12 (R1), 0.86 ± 0.20 (R2), 0.87 ± 0.29 (R3), 2.22 ± 0.99 mg/L/d (R4), and the V_{max} were 173.99 ± 14.06 (R1), 235.20 ± 24.40 (R2), 347.44 ± 51.50 (R3), 409.02 ± 108.94 mg/L (R4), respectively. Aeration rates significantly influenced the kinetic parameters (K_m and V_{max}) of the bioreactors. The K_m and V_{max} values of the bioreactor with high aeration rate were higher than those of the bioreactor with low aeration rate, indicating enhanced microbial activity and substrate utilization.

In Table S2, the oxygen affinities (oxygen half-full and constant) of ammonia-nitrite-oxidizing bacteria and nitrite-oxidizing bacteria are generally recognized as 1–40 μM (0.014–0.56 mg/L/d) [26–29] and 4.06–16.88 μM (0.05684–0.23632 mg/L/d) [26,30–32], while that of non-oxygenophilic heterotrophic bacteria is only 0.00312 μM (0.00004368 mg/L/d) [33]. Tsukamoto et al. [16] suggested that ammonia loss could be inhibited by reducing dissolved oxygen and maintaining heterotrophic ammonia recovery at low DO. However, its limited heterotrophic microbial activity cannot achieve complete ammonia assimilation and efficient nitrogen recovery performance. Aerobic heterotrophic ammonia-assimilating bacteria have low oxygen affinity, resembling NOB (lower oxygen affinity) more than AOB (higher oxygen affinity), thus require sufficient dissolved oxygen to support efficient assimilation.

3.3. Microbial metabolic compounds

3.3.1. Soluble microbial products

The EEM spectra of SMP samples were characterized in Figure S5. The main peaks of components 1, 2 and 3 of SMP were separated by PARAFAC model (Fig. 2 A-C). Component 1 was at excitation/emission (Ex/Em) 275/350 nm (peak a) and 230/340 nm (peak b), corresponding to tryptophan and aromatic protein-like substances. Peaks c and d at 275/310 nm and 230/310 nm were identified as tyrosine protein-like and tryptophan protein-like substances in component 2 of SMP [8]. In component 3, peaks e and f at 340/420 nm and 275/420 nm were identified as humic and fulvic acid-like substances. The different initial ratios of components across R1–R4 at 0 h were attributed to pre-existing microbial metabolic heterogeneity resulting from prior adaptation of the corresponding sludge to distinct aeration rates during long-term reactor operation. In the R1 and R2 bioreactors (Fig. 2 D-G), the maximum fluorescence intensity proportion of component 1 decreased from 47.5 % and 65.0–27.0 % and 30.8 %, respectively, while component 2 increased from 31.8 % and 21.5–48.5 % and 46.2 %. Component 3 did not fluctuate much in the R1 and R2 bioreactors. Tyrosine protein-like and tryptophan protein-like substances were consumed in the form of more generation and transformation of tryptophan and aromatic protein-like substances in microbial metabolism due to the low dissolved oxygen environment. In contrast, bioreactors in high dissolved oxygen environments showed the opposite trend. In R3 and R4 bioreactors, the proportion of component 1 increased from 30.7 % and 35.7–50.3 % and 47.6 %, respectively, while the proportion of component 2 decreased from 54.3 % and 51.0–33.6 % and 23.5 %. At the end of the reaction in the R4 bioreactor, component 3 suddenly increased from 8.6 % to 28.8 % with the decrease of components 1 and 2, possibly due to excess aeration and nutritional deficiencies caused by cell residue accumulation [13]. FRI analysis (Figure S7) showed that soluble microbial by-product-like substances (Region IV) dominated across all reactors. R2 and R3 exhibited marked declines in protein-like regions (I–II) and increases in humic-like substances (Region V), suggesting progressive microbial humification. R4 maintained stable fluorescence, indicating enhanced organic stabilization under higher aeration. These trends highlight oxygen-driven transformation from labile to recalcitrant organics [21].

3.3.2. Extracellular polymeric substances

The electrochemical properties of EPS were analyzed using CV curve and EIS test (Fig. 2 H-I). In the CV curves, redox peaks were observed in all reactors, indicating that redox-active compounds in EPS participated in electron transfer. Higher peak currents were recorded in reactors with increased aeration rates, suggesting that microbial electron transfer activity was enhanced under these conditions. The results of EIS analysis showed that the EPS of the highly aerated bioreactor sludge had higher electron transfer capacity, suggesting stronger organic oxidation and utilization capacity. In addition, the PN and PS content of EPS in the four bioreactors was compared to evaluate the impact of aeration on extracellular matrix composition (Fig. 2 J). From the perspective of sludge extracellular metabolites, the bioreactor with higher dissolved oxygen supply had more protein content, suggesting that elevated DO levels potentially enhanced microbial activity and structural stability of the biofloc. The reactor with higher aeration rate exhibited increased protein content and reduced PS/PN ratios, which likely contributed to improved flocculation and sedimentation performance. These conditions promoted the formation of compact and robust biofilms, thereby enhancing microbial resistance to shear stress and supporting stable reactor operation. Conversely, higher PS fractions in low-aeration system may lead to looser biofloc structures, reducing sludge settleability.

3.3.3. Assimilative key substances

The GDH, GOGAT, and GS are key enzymes in this process, responsible for catalyzing the incorporation of ammonia into α-ketoglutarate to form Glu, and further conversion of Glu into Gln (Fig. 3A). Although the metabolic pathway prediction was based on 16S rRNA gene sequences using PICRUSt2, its accuracy is supported by previous benchmarking studies [34] and corroborated by metagenomic evidence from halophilic nitrogen-assimilating microbiomes in saline wastewater systems [3], which consistently identified key genes such as *glnA*, *gltB*, and *gdhA* involved in ammonia assimilation. The activity ranges of GDH, GOGAT and GS were 56.53–85.85 mU/g MLSS, 987.06–2673.40 U/g MLSS and 19.77–88.71 U/g MLSS, respectively. The enzyme activity of GOGAT (43.02–170.84 %) and GS (183.47–348.70 %) increased significantly, while the activity of GDH (4.88–51.87 %) changed little. Nitrogen metabolism in the system relied more heavily on the GS-GOGAT cycle for ammonia assimilation. TAA was above 240 mg/g MLSS. In addition, Glu and Gln content fluctuated between 7.90 % and 11.21 % and 8.72 ~ 12.33 % of TAA content. In aerobic metabolism, electrons in the respiratory chain were transferred from NADPH and ATP to the corresponding electron acceptor reductase to facilitate proton transport across the membrane to form proton power and ultimately to produce energy. With the increase of aeration rate, ATP increased from 0.68 μmol/g MLSS (0.1 L/min·L) to 2.92 μmol/g MLSS (3 L/min·L), while NADPH increased from 2.16 μmol/g MLSS (0.1 L/min·L) to 4.82 μmol/g MLSS (3 L/min·L). Oxygen also affected the ammonia assimilation efficiency by affecting the synthesis of NADPH and ATP.

3.3.4. Functional gene prediction based on KEGG

PICRUSt-based KEGG pathway analysis was applied to high-throughput sequencing data, revealing insights into carbon and nitrogen metabolism (Fig. 3B). In the pathway of nitrogen assimilation metabolism, the proportion of *glnA* gene was at a high level, ranging from 0.107 % to 0.123 %. Other ammonia assimilation genes were also at relatively high levels, such as *gdhA* (0.051–0.070 %), *GLUD* (0.021–0.024 %), *glnE* (0.035–0.038 %), *gltD* (0.050–0.056 %), and *gltB* (0.040–0.042 %). The increase of aeration intensity decreased the gene expression of the GDH pathway (*GLUD*, *gdhA*) and promoted the GOGAT pathway genes, possibly because DO enhance the synthesis activity of ATP and NADPH, which led to more ammonia switching to GS pathway for assimilation. Nitrification gene *hao* was present at low levels (<

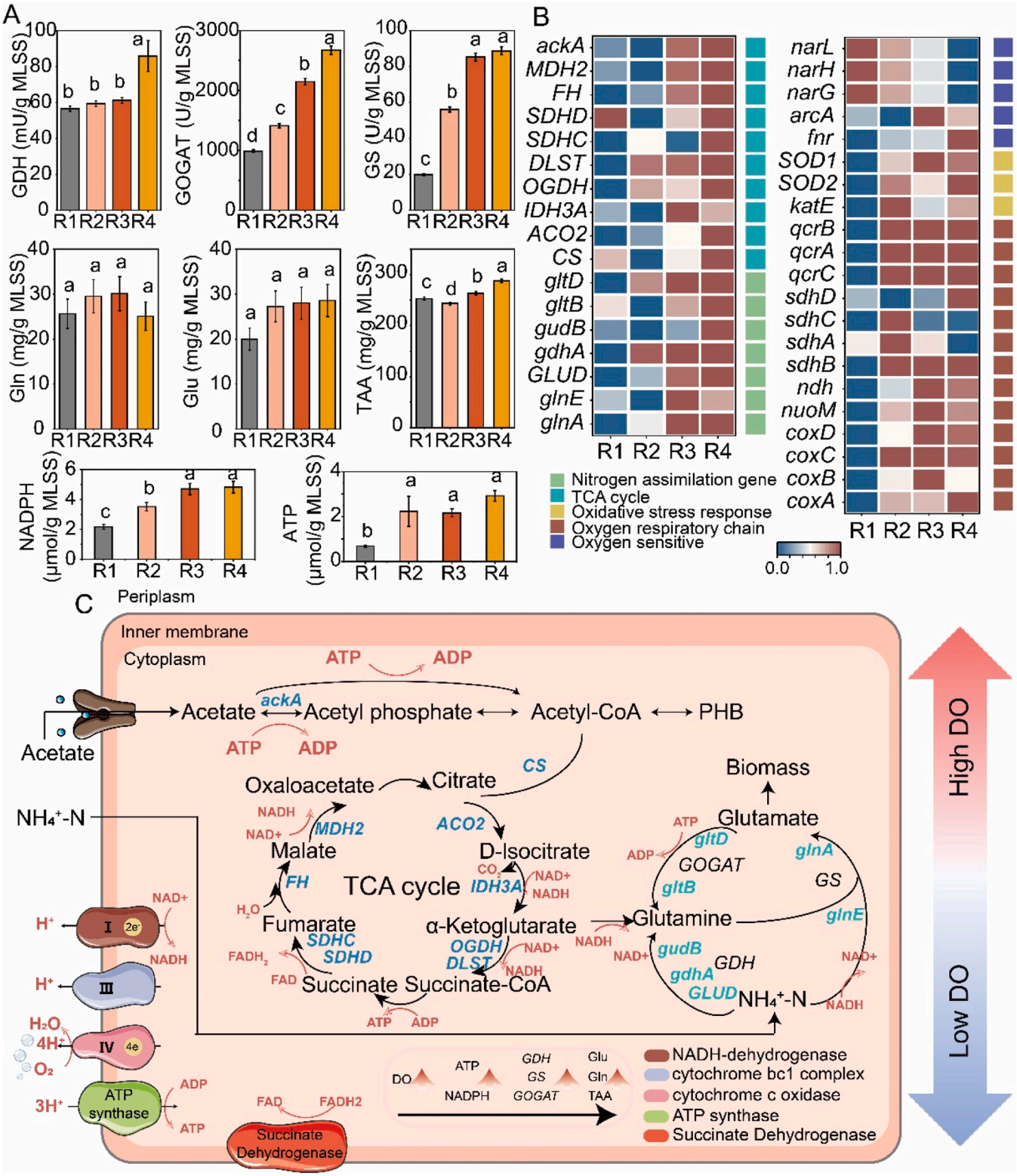

Fig. 3. Mechanism analysis: (A) The enzyme activity, amino acids and energy molecules of assimilation pathways; (B) The relative abundances of the nitrogen and carbon genes predicted by PICRUSt; (C) The metabolic diagram. Different lowercase letters (a, b, c, etc.) indicate statistically significant differences ($p < 0.05$) among groups based on one-way ANOVA followed by Tukey's post hoc test.

10^{-4}%) and *amoA* was undetected, confirming the absence of nitrification.

In TCA cycle, the stimulation of dissolved oxygen also increased the expression of various functional genes. In particular, the genes of citric acid synthetase (*CS*) and Isocitrate Dehydrogenase (*IDH3A*) were significantly up-regulated, which were indispensable for the synthesis of alpha-ketoglutaric acid [3]. Similarly, there was a consistent trend in other pathway genes involved in NADPH conversion responses, such as *OGDH*, *DLST*, *SDHC/D*, and *MDH*$_2$. Bacteria perform oxygen utilization and electron production through oxidases on the biofilm. Aerobic

respiration involves key genes such as *coxA*, *coxB*, and *coxC*, which encoded subunit of cytochrome c oxidase, facilitating the transfer of electrons to oxygen, the terminal electron acceptor. Genes like *nuo* and *sdh* encoded components of the electron transport chain, enabling efficient energy production via oxidative phosphorylation. The expression of these genes increased with the increase of oxygen load. The O_2 has a high REDOX potential ($\Delta E^{\cdot}_0 = +0.82$ V), and each reduction of oxygen molecules will produce four protons across the membrane into the membrane gap [7]. In oxidative stress conditions, bacteria activate antioxidant defense mechanisms. The *katE*, *SOD1* and *SOD2* were up-regulated with the increase of aeration rate. The increase of oxygen content led to the activation of microbial self-protection mechanisms

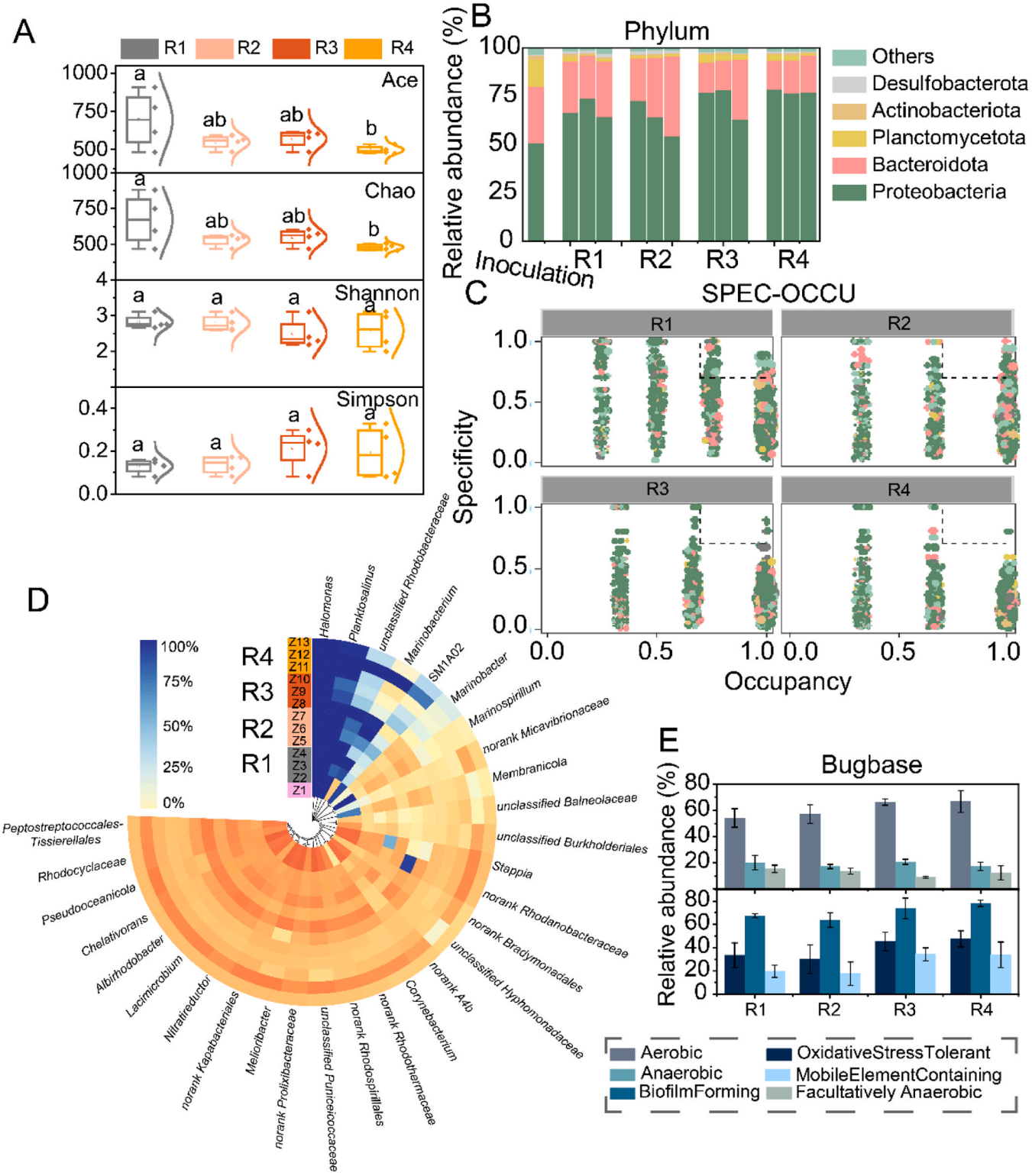

Fig. 4. Microbial community: (A) The alpha indices, including chao, sobs, shannon and simpson index. Microbial community at (B) phyla level and (D) genus level. The (C)SPEC-OCCU and (E) BugBase plots for potential keystone species identification and bacterial phenotype prediction. Different lowercase letters (a, b, c, etc.) indicate statistically significant differences ($p < 0.05$) among groups based on one-way ANOVA followed by Tukey's post hoc test.

such as superoxide dismutase (SOD), which reduced harmful substances reactive oxygen species (ROS) to oxidized glutathione (GSSG), thereby avoiding ROS damage to cells [35]. Regulatory genes like *fnr*, *arcA* and *arcB* coordinate the transition between aerobic and anaerobic states, revealed the versatility of bacterial metabolism in adapting to fluctuating oxygen levels, balancing energy production and protection against oxidative damage.

3.3.5. Nitrogen assimilation mechanism analysis

The simplified metabolic network based on the process of heterotrophic ammonia assimilation is shown in Fig. 3C. The acetate was involved in the TCA cycle as a carbon driver, providing the electrons involved in the NADPH synthesis, as well as the α-ketoglutaric acid required by HAA. Oxygen entered the cell through respiration and metabolism to produce water and carbon dioxide to produce electrons, thereby maintaining basic cell metabolism and growth. Oxygen acted as the final electron acceptor in the electron transport chain, enabling the production of ATP through oxidative phosphorylation. In HAA metabolism, ammonia and α-ketoglutaric acid were synthesized to glutamate under GDH enzyme, stands out because it does not require ATP or NADPH, led the HAA pathway less susceptible to fluctuations in DO levels. In GOGAT/GS pathway, glutamine and ammonia synthesis of glutamate under the support of ATP and NADPH, as well as the regeneration of glutamine were two biomass synthesis reactions under high nutrient conditions. The reliance on ATP and NADPH made the GOGAT/GS pathway more resource-intensive. Adequate oxygen levels were necessary to support the energy demands of these processes. Oxygen limitation can hinder the GOGAT and GS processes, potentially slowing down cell growth and affecting overall metabolic efficiency.

3.4. Microbial community

The oxygen intensity profoundly affected the survival, metabolism and reproduction of microorganisms with different degrees of oxygen affinity, thus affecting different aspects of microbial communities in bioreactors. The ACE, Chao and Shannon values of microbial samples in bioreactors with higher aeration rate were lower, while Simpson values showed an opposite trend (Fig. 4A). Similarly, Venn analysis built on OTU numbers shows a similar trend (Figure S8). The enhanced aeration supply reduced the number of sample species and community diversity, thereby improving the functionality of obligate microbial populations for survival in aerobic states.

At phylum level (Fig. 4B), the relative abundance of Proteobacteria in bioreactors was as high as 57.3–64.0 %. Proteobacteria was the main promoter of heterotrophic ammonia assimilation reaction [7], and participates in nitrogen and carbon cycle, which had high ecological value [36]. The abundance of Bacteroidota ranged from 23.1 % to 30.3 %. Higher aeration rates correspond to higher Planctomycetota abundance and less Desulfobacterota. The Specific-Occupancy (SPEC-OCCU) method identifies core microbial taxa by evaluating their specificity and occupancy across samples, helping to highlight functional keystone organisms under different environmental conditions. In Fig. 4C, the relevant taxon based on SPEC-OCCU showed that 37, 37, 4, and 1 functional microbial phylum ($0.7 < \text{Specificity} < 1.0$, $0.7 < \text{Occupancy} < 1.0$) had been identified as key taxa of R1, R2, R3 and R4 bioreactors, respectively [37]. Higher the aeration rate, more the key microbial phylum number. The abundance of Proteobacteria accounted for more than 30 % in the key phylum.

At genus level (Fig. 4D), *Halomonas*, as the dominant microorganism with the highest abundance, increased from 12.77 % (inoculation) to 28.51 % (R1), 22.67 % (R2), 47.92 % (R3) and 43.09 % (R4) in the inoculated sludge, respectively. *Halomonas* can improve the synthesis of intracellular substances by increasing the levels of ATP, NADH/NAD^+ and oxygen utilization [38]. Similarly, this genus was one of the major contributors to the nitrogen recovery process of the heterotrophic ammonia assimilation process. *Planktosalinus*, as an important HAA functional bacterium, increased from 16.48 % (inoculation) to an average of 19.95 % (R1) and 25.80 % (R2), and decreased to an average of 15.85 % (R3) and 15.85 % (R4). The results showed that this genus was adapted to enrich in low and medium dissolved oxygen environment, but was inhibited by stress under high dissolved oxygen environment [8]. In particular, the abundance of *Marinobacterium* had increased dramatically from 1.69 % (inoculation) to 11.69 % (R1), 11.03 % (R2), 3.17 % (R3) and 6.05 % (R4). There was a literature showing that it can effectively degrade refractory organic matter in saline wastewater under the condition of micro-aeration [39]. Notably, no microorganisms with autotrophic nitrification were detected in any of the four aeration-supplied HAA bioreactors. The Bugbase predicts microbial phenotypes (e.g., aerobic, anaerobic, pathogenic traits) from 16S rRNA data using a reference database, allowing inference of community-level traits under different conditions. The Bugbase phenotypic predictive function analysis was established to investigate the effect of aeration rate on phenotypic transformation of HAA microbial communities (Fig. 4E). In the predicted information, the abundance of aerobic bacteria was higher in the bioreactor with higher aeration rate, while the anaerobic and facultatively anaerobic bacteria showed opposite trends. In addition, oxidative stress tolerant bacteria were significantly different, with abundances of 33.43 % (R1), 30.02 % (R2), 45.32 % (R3) and 47.55 % (R4), respectively. The impact of different aeration rates on microbial populations, driving the selective enrichment and proliferation of specific functional microorganisms.

3.5. Microbial network analysis and assembly mechanisms

Microbial co-occurrence networks are constructed based on pairwise correlations, revealing potential interactions, cooperation, or competition among microbial taxa in complex communities. The cooccurrence network (Fig. 5 and Table S3) based on R1, R2, R3 and R4 microbiomes consisted of 334, 345, 273, 261 nodes and 3697, 4224, 2552, 2177 edges, respectively. The modularity degrees were 0.854, 0.819, 0.781 and 0.796, respectively, and the average degrees were 22.138, 24.487, 18.696 and 16.682, respectively. The positive correlations between co-occurring networks were 74.55–81.23 %. Fig. 5A showed the co-occurrence network of R1 bioreactor, which was mainly composed of five modules, accounting for 11.7 %, 11.4 %, 11.1 %, 10.8 % and 6.3 % of all microorganisms, respectively. *Stappia* and *Marinospirillum*, the removal contributors of refractory organic matter [3,40], such as phenol and azo dyes, dominated module 1 and module 4. However, the two genera with the largest abundances *Halomonas* and *Planktosalinus*, were not in the main modules. The co-occurrence network of R2 bioreactor (Fig. 5B) consisted of module 1 (15.7 %), module 2 (11.9 %), module 3 (9.6 %), and module 4 (6.7 %). Under slightly higher DO conditions, *Azohydromonas* of module 1 can generate high value polyhydroxybutyrate in excess [41]; *Geobacter* of module 2, had unique functions in electron transfer and energy recovery [13]; *Salinicoccus* of module 3 can enhance ROS homeostasis and detoxification metabolism under high salt [42]. In the co-occurrence network of R3 bioreactor (Fig. 5C), module 1 (17.2 %) was the dominant module, which was formed by the cooperation and competition of various bacteria genera such as *SM1A02*. In addition, *Brevundimonas* in module 2, *Mariniphag* in module 3, and *unclassified_Rhodobacteraceae* in module 4 all had positive interactions with other bacteria. *Brevundimonas and Mariniphag* had an extremely strong tolerance to stress [43], while *unclassified_Rhodobacteraceae* was considered to have organic metabolism capacity [44]. In Fig. 5D, modules 1 and 2 formed the microbial network of the R4 bioreactor with the highest aeration rate. Among them, *Halomonas* and *Gelidibacter* [45] of module 1 had mutually reinforcing effects in terms of nitrogen removal. Module 2 contained *norank_Micavibrionaceae* and all its relationships were positive interactions. The within-module connectivity (Zi) and among-module connectivity (Pi) values measure a topological role of taxon in a network, distinguishing module hubs (high Zi) and connectors (high Pi) important for microbial community

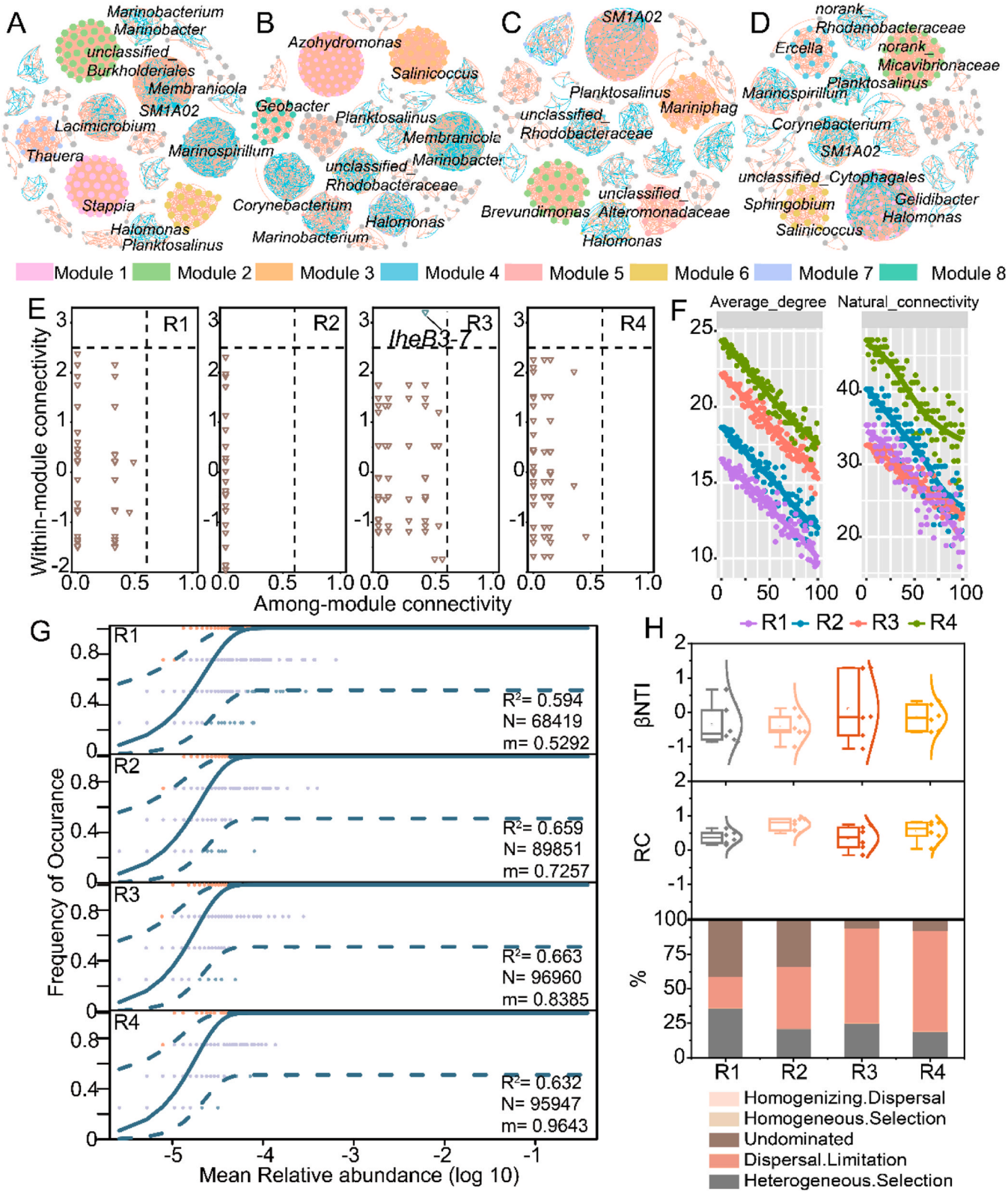

Fig. 5. In-depth analysis of microbial communities from bioreactor sources supplied by different carbon sources: Microbiome co-occurrence network in (A) R1, (B) R2, (C) R3, (D) R4 bioreactors. (E) The Z-P plot of species topological roles. (F) Robustness analysis based on the average degree andnatural connectivity of six microbial networks. (G) Fit of neutral community model (NCM) of community assembly. (H) Distribution of beta nearest taxon index (βNTI), Raup-Crick metric (RCbray), and contributions of deterministic and stochastic processes evaluated by null model framework. A blue line in the networks indicated significant positive interactions, and a red line indicated significant negative interactions.

structure and stability. The Zi and Pi were assessed (Fig. 5E), revealing that 99.9 % of nodes were classified as Peripheral nodes. Only one Module hub had been found in the R3 bioreactor, *IheB3–7* (Family *Melioribacteraceae*) [46], which was considered to be the dominant bacterium at slightly higher DO level [47]. Its presence under high-salinity and oxygen-rich conditions may point to involvement in organic matter degradation or redox-sensitive metabolic processes [47]. *Iheb3–7* may share metabolic intermediates with other bacteria in a

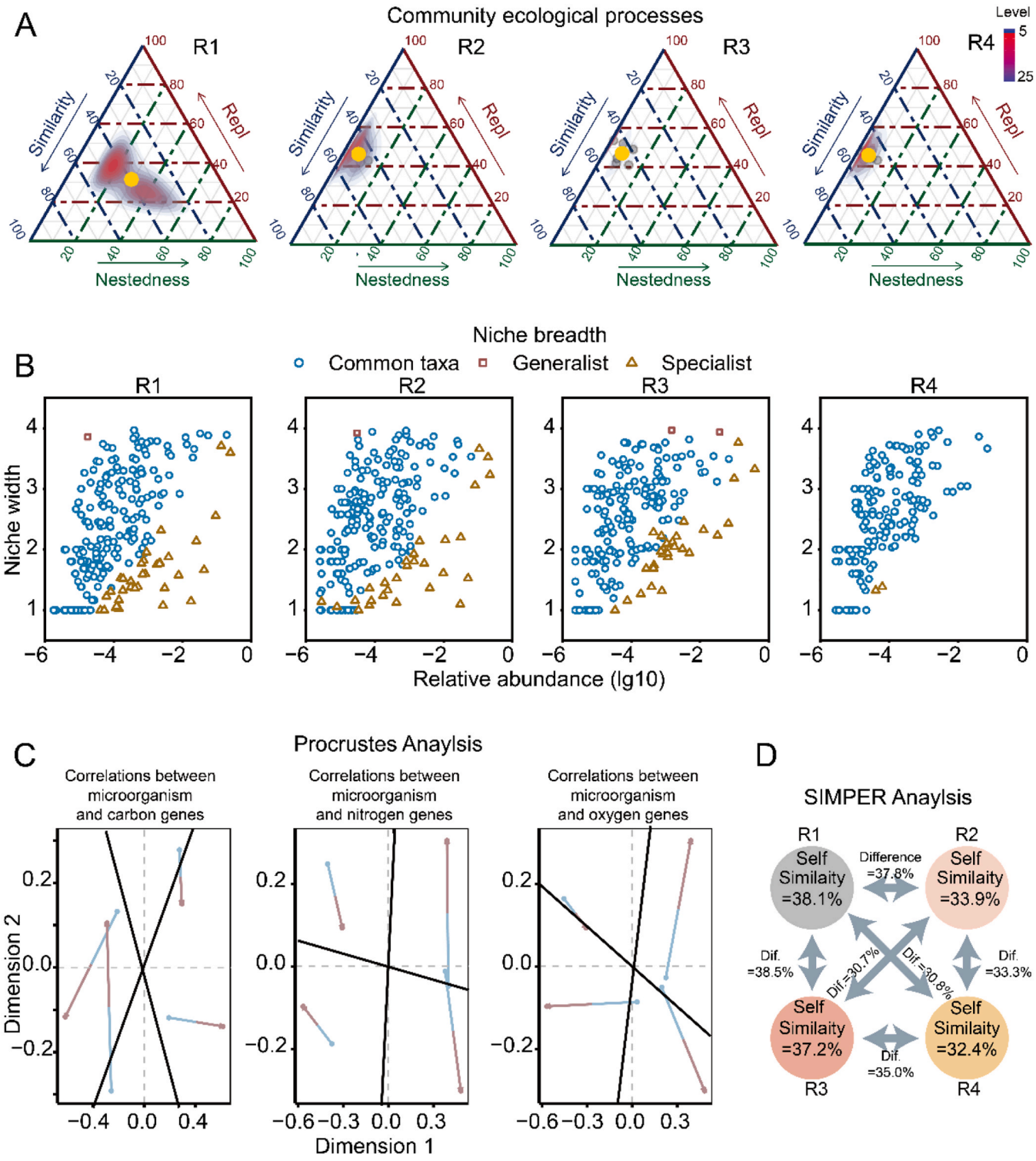

Fig. 6. The self-assembly process of microbial communities: (A) Triangular plots show community ecological processes (i.e., species substitution and richness differences) of bacteria in the four bioreactors. Its position is denoted by a triplet of values from the Similarity = 1 – dissimilarity, Repl (replacement), Nestedness; each triplet sums to 1. (B) Niche breadth of the generalists and specialists. Relative abundance was shown on a logarithmic (lg) scale. (C) Pairwise correlation analyses based on the Bray-Curtis matrix for nitrogen, carbon, oxygen genes and microorganism using Procrustes analysis, microorganism-nitrogen genes, microorganism-carbon genes, and microorganism-TPHs genes. The forward path coefficients are indicated by red arrows. (D) Similarity Percentage (SIMPER) of microbial communities.

positive way [6], thus exerting the network cohesion function of Module hub. Robustness analysis evaluates the stability of microbial networks by measuring parameters like natural connectivity and resistance to node removal, indicating ecosystem resilience to disturbance. In robustness analysis (Fig. 5F), the microbial communities of bioreactors with higher aeration rates showed higher robustness. The proportion of network complexity and positive correlation in the four bioreactors was positively correlated with the stability, and the establishment of a more stable community network may depend on the enrichment of dominant species in an aerobic environment [21]. After the initiation of ammonia assimilation, an adequate oxygen environment limited the further spread of non-dominant species, providing support for the preferential effect [48].

The Sloan NCM assesses the contribution of stochastic processes (e.g., dispersal, drift) in microbial assembly by comparing observed species distributions to those predicted by neutral theory. In NCM analysis (Fig. 5G-H), the N values of R1-R4 bioreactors were 68,419, 89,851, 96,960 and 95,947, respectively, indicating that higher aeration rates led to random selection playing a more important role in microbial community construction. The m value had a consistent change trend, revealing that the microbial community with higher aeration rate may have a higher migration rate and less dispersal limitation [49]. These results highlight that stochastic community assembly under higher aeration may facilitate the ecological adaptation of HAA systems to fluctuating oxygen conditions. Null model analysis quantifies the relative influence of deterministic versus stochastic processes in microbial community assembly using βNTI and RC metrics to infer ecological drivers. Null model analysis (Fig. 5H) was performed to evaluate the relative contributions of deterministic and stochastic processes under varying aeration rates. The βNTI and RC values, consistently within the range of −2 to 2, confirmed that stochastic processes predominantly governed community assembly [8]. The higher aeration rate led to the higher proportion of Dispersal Limitation and the lower proportion of Heterogeneous Selection and Undominated on the community assembly. The self-assembly of HAA microorganisms under varying aeration rates was primarily influenced by stochastic processes, with higher aeration rate increasing random selection, migration, and dispersal limitation, although deterministic factors still played a role. This suggests that aeration-driven stochastic processes play a key role in shaping microbial compositions critical for efficient ammonia assimilation. Moreover, the ternary plots (Fig. 6A) indicated that community assembly was shaped by both stochastic and deterministic factors, with varying levels of similarity, nestedness, and replacement across reactors (R1–R4). Such variations reflect the flexible microbial adaptation strategies supporting sustained nitrogen conversion in HAA systems. Niche breadth analysis estimates how widely taxa are distributed across environmental gradients, distinguishing generalists (broad niches) from specialists (narrow niches) based on Levin's index. Niche breadth analysis (Fig. 6B) showed that generalists had broader ecological niches and higher abundance, indicating their adaptability to DO fluctuations. Specialists, in contrast, exhibited narrow niches and lower abundance, suggesting their preference for stable conditions, revealed the functional differentiation of microbial community in response to oxygen availability. This ecological differentiation is closely related to the microbial community's ability to maintain nitrogen assimilation across varying aeration intensities. Procrustes analysis compares two multivariate datasets (taxonomy vs. gene function) by superimposing them to evaluate concordance between microbial composition and functional profiles. Procrustes analysis (Fig. 6C) revealed strong correlations between microbial composition and nitrogen-related genes, suggesting that nitrogen metabolism played a crucial role in community structuring. The correlation with oxygen genes further supported the impact of DO on microbial functional capacity. SIMPER analysis identifies the microbial taxa contributing most to community dissimilarity between groups, quantifying their relative impact on compositional variation. SIMPER analysis (Fig. 6D) indicated that self-similarity varied among reactors, with the highest in R1 (38.1 %) and the lowest in R4 (32.4 %), emphasizing the significant shifts in microbial communities due to DO variations. This microbial divergence further supports the hypothesis that aeration intensity modulates functional microbial specialization for ammonia assimilation.

The observed shifts in microbial community structure under varying oxygen intensities can be explained by the interplay of ecological niche theory and neutral theory. Differences in oxygen affinity among microorganisms led to niche partitioning, where high oxygen concentrations favored obligate aerobes with efficient respiration and antioxidant systems, enhancing nitrogen assimilation. Conversely, facultative and microaerophilic taxa were outcompeted at elevated DO, leading to reduced diversity but increased specialization. This pattern reflects ecological filtering, where environmental constraints such as DO selectively enrich functionally advantageous populations while excluding less competitive taxa. However, despite the clear influence of deterministic selection, stochastic processes dominated the overall community assembly, as supported by neutral theory [50]. Similar trends of stochastic dominance have been reported in microbial communities exposed to salinity and oxygen gradients, where dispersal limitation increases under environmental disturbance. Compared with stable wastewater systems, the dynamic aeration regime in this study likely intensified random assembly by continuously disrupting microbial equilibrium. The coexistence of functional specialization with stochastic structuring suggests that while aeration filters for key functional groups, it simultaneously promotes random turnover of the broader community. These findings provide ecological insight into the balance between deterministic selection and stochastic drift in engineered systems, emphasizing that aeration regulation influences not only pollutant removal but also the ecological mechanisms shaping microbial assembly.

3.6. Energy consumption and nitrogen footprint

Nitrogen footprint, as an index to quantitatively analyze the impact of wastewater treatment on reactive nitrogen emission and water resources, provided a new theory and approach for evaluating the environmental effect of nitrogen-containing wastewater utilization system. The total nitrogen footprint (NF_{TOT}) comprised effluent residual nitrogen (NF_{wat}), air emissions (NF_{air}), sludge generation (NF_{slud}), and electricity use (NF_{elec}) (Fig. 7A and B). NF_{wat} decreased with increasing aeration rates, indicating better nitrogen removal efficiency at higher DO levels. Conversely, NF_{slud} increased significantly, especially at R3 and R4, due to enhanced microbial activity and biomass generation. Because nitrogen was removed through the heterotrophic ammonia assimilation pathway rather than oxidized to gaseous form, it is considered that the nitrogen removal in the nitrogen oxide form (NF_{air}) was approximately zero. The contribution of NF_{elec} became prominent at high aeration rates due to increased energy demand. Excessive aeration leaded to a sharp increase in NF_{TOT} due to higher energy-related emissions.

The different aeration rates led to different aeration pump energy consumption (Fig. 7C). Under the same energy consumption of the inlet and outlet pumps, the specific energy demand (SED) of R1-R4 bioreactors were 0.0038, 0.0126, 0.0236 and 0.0676 kWh/d, respectively. Aeration energy dominated the total energy demand compared to filtration, especially at higher aeration rate, where aeration contributed over 95 % of total energy consumption. Based on this, the pollutant removal efficiencies and the aeration cost were combined to obtain the optimal aeration rate (Fig. 7D). Obviously, the aeration rates of 1–3 L/min·L were considered as the parameter range of optimal pollutant removal. The optimal aeration rate is 1 L/min·L, where high efficiency is achieved with moderate energy input, aligning with sustainable operation goals.

From a practical perspective, R3 exhibited the best balance between nitrogen removal efficiency and energy cost, making it promising for

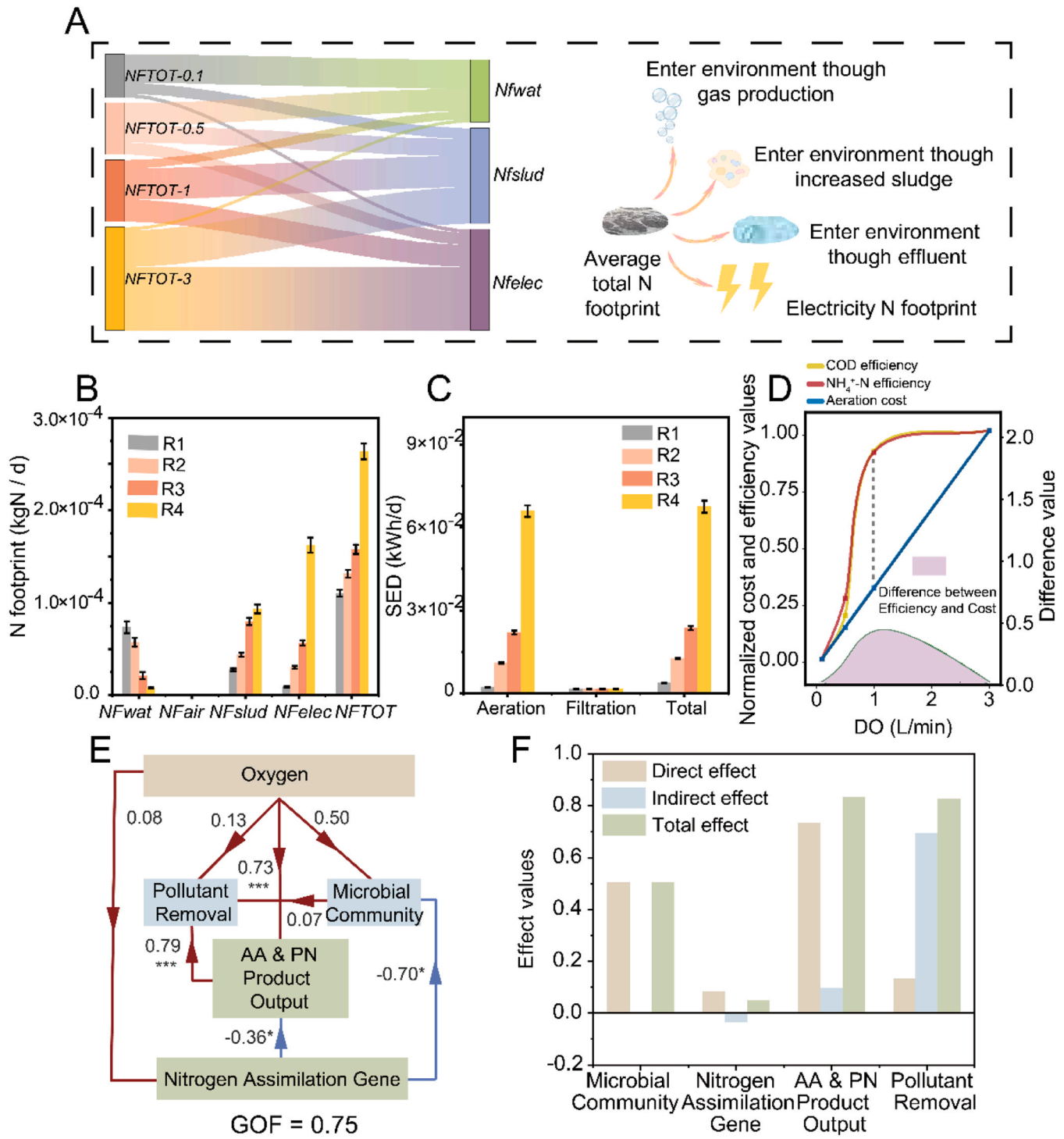

Fig. 7. Energy consumption, carbon emissions, and nitrogen footprint: (A) Sankey diagram of energy consumption, carbon emissions, and nitrogen footprint. in bioreactors. The content comparison of (B) nitrogen footprint and (C) energy consumption. (D) Optimal aeration rate curve based on efficiency and energy consumption. (E) Partial least-squares path model (PLS-PM) of relationships between oxygen, microbial community, pollutant removal, nitrogen assimilation gene, and AA & PN product output. (F) Standardized total, direct and indirect effect values calculated by PLS-PM. (*p < 0.05; *p < 0.01, ***p < 0.001).

engineering-scale application. However, further techno-economic analysis is needed to assess long-term operating costs and return on nutrient recovery. In addition, environmental indicators beyond nitrogen, such as COD utilization, sludge production, and potential carbon emissions, should be integrated into future life-cycle assessments to provide a more comprehensive sustainability profile.

3.7. Contribution calculation and correlation analysis

Fig. 7F and G show the contribution relationship and standardized total effect analysis of oxygen load, pollutant degradation, microbial community, functional genes, and protein production in bioreactors using PLS-PM. Variable selection was based on a combination of biological relevance, variance contribution, and meaningful ecological factors (e.g., functional microorganism abundance, key functional

genes, nitrogen removal metrics). It is noted that PLS-PM is a correlation-based method and does not establish causality. Therefore, the identified pathways should be interpreted as potential associations that support mechanistic hypotheses but require further experimental verification. The goodness of fit value of 0.75 indicated that the model had good adaptability. The oxygen load had a positive relationship with the four main aspects. The total contribution value of oxygen load to the four factors was also positive, which was 0.83 for pollutant degradation, 0.50 for microbial community, 0.05 for functional genes and 0.83 for protein production. In addition, oxygen load showed a highly significant positive relationship on pollutant removal ($p < 0.001$). The correlation analysis of system performance with functional genes and functional bacteria (Figure S9). The NH_4^+-N removal and oxygen load were highly correlated with nitrogen function genes ($0.001 < p \leq 0.01$), indicating that oxygen intensity significantly affected microbial community structure and microbial nitrogen transformation in HAA systems. Future research should focus on further optimizing aeration strategies and exploring the long-term impacts on microbial communities and treatment performance.

3.8. Significances and prospects

Oxygen driven HAA process enhanced wastewater treatment sustainability and environmental friendliness. Although the supply of sufficient oxygen and carbon sources may be more prominent in the single-stage process energy consumption, HAA avoided the problem of intermittent oxygen supply and unreasonable organic carbon supply from the perspective of the long chain of sewage treatment, thus realized the recovery of nitrogen resources without producing harmful intermediates. In terms of full chain cost and environmental significance, HAA had advantages over existing wastewater treatment processes, especially high-salinity wastewater. HAA process produced partial high value-added sludge due to the accumulation of nutrient products, which had higher nitrogen content and activity than the existing wastewater treatment process sludge [3,8], thus became the best raw material for sludge resource treatment. Compared with previous studies on saline wastewater treatment [14,17,51–53], this work provides a more systematic understanding of how aeration precisely regulates heterotrophic ammonia assimilation, achieving high NH_4^+-N and COD removal efficiencies (>94 %) while promoting the dominance of halophilic functional taxa. Unlike conventional nitrification-denitrification or partial nitrification processes, our study emphasizes aerobic assimilation pathways and microbial network reinforcement, offering a novel ecological strategy for stable and efficient nitrogen recovery under hypersaline stress. The high value-added HAA sludge was considered a resource rather than a waste, and can also be applied to the soil as a microbial fertilizer after harmless treatment [3], thus minimizing nitrogen losses from side stream recycling. Detailed, the direct regulation of biofilm EPS by salt-tolerant microorganisms enhances soil structural integrity, offering a viable strategy for improving soil aggregates [54]. Unique assimilative metabolic pathways in HAA further contribute to soil organic carbon pump formation and restoration while retaining nitrogen, a mechanism currently under investigation by our team.

The successful establishment of salt-tolerant HAA communities in this study was attributed to the use of marine sediment-derived microorganisms as inoculum sources combined with targeted domestication strategies. Ensuring that only ammonia assimilation occurs without nitrification in full-scale systems remains challenging. Key control factors may include competitive inhibition of nitrifying bacteria by dominant heterotrophic communities, strict regulation of the influent C/N ratio, and salinity-induced selective pressure that favors heterotrophic metabolism over autotrophic pathways. However, the relative contribution of each control factor and their interactions require further investigation. For large-scale applications, dedicated inoculation and enrichment systems will need to be developed, including process equipment specifically designed for the domestication of halophilic heterotrophic populations.

While the study demonstrates the efficiency of HAA in nitrogen recovery and sludge valorization, future work should address key engineering challenges. These include developing low-energy oxygen delivery systems that can maintain optimal DO levels identified in this study (e.g., R3 conditions), and designing reactors that support stable biofilm structure and oxygen transfer under saline conditions. Developing low-energy, fine-tuned aeration systems that can maintain optimal DO without over-aeration is essential. Reactor design must address the dual needs of effective biomass retention and oxygen transfer, especially under saline conditions. Moreover, long-term field trials are needed to assess the agronomic value and environmental safety of HAA sludge when applied to saline-alkali soils. These targeted efforts will facilitate the transition of HAA from bench-scale success to full-scale implementation. Future research will aim to advance more efficient sludge management strategies, fostering novel pathways for resource recovery and environmental sustainability.

4. Conclusions

This study investigated the effects of aeration rates on HAA bioreactors, focusing on performance and microbial dynamics. Higher aeration significantly improved NH_4^+-N and COD removal, stabilized operations, enhanced biomass growth, and optimized substrate utilization. Batch tests confirmed HAA as the primary nitrogen removal pathway. Microbial analysis revealed that increased aeration reduced diversity and species richness, favoring *Halomonas* dominance. Ecological analyses revealed that stochastic processes governed microbial community assembly under aeration-driven selective pressures, balancing random dispersal with functional specialization. Additionally, nitrogen footprint analysis demonstrated that HAA effectively reduced reactive nitrogen emissions by transforming ammonium into biomass, eliminating gaseous nitrogen loss while promoting resource recovery. The optimal aeration rates were 1–3 L/min·L, with 1 L/min·L offering the best balance between efficiency and cost. These findings provide valuable insights for optimizing wastewater treatment, improving pollutant degradation, and advancing sustainable environmental management strategies.

CRediT authorship contribution statement

Fei Han: Data curation. **Mengru Zhang:** Data curation. **Yuke Li:** Writing – review & editing. **Weizhi Zhou:** Writing – review & editing, Supervision, Funding acquisition. **Chuanfu Zhao:** Writing – original draft, Data curation. **Wenhao Zhang:** Data curation. **Yiting Guo:** Data curation.

Declaration of Competing Interest

The authors declare that they have no known competing financial interests or personal relationships that could have appeared to influence the work reported in this paper.

Acknowledgments

This work was supported by National Key R&D Program of China (2022YFC2807503); National Natural Science Foundation of China (U1906221).

Appendix A. Supporting information

Supplementary data associated with this article can be found in the online version at doi:10.1016/j.jece.2025.117911.

Data availability

Data will be made available on request.

References

[1] C. Zhao, W. Zhang, Y. Guo, M. Zhang, F. Han, J. Lei, W. Zhou, Flocculent sludge outperforms filler biofilm for high salinity oilfield produced water treatment: performance, metabolic pathways, and microbial communities, J. Hazard Mater. 492 (2025) 138217.

[2] C. Zhao, S. Meng, L. Yan, X. Zhang, Q. Wei, D. Wei, Coupling of submersible microbial fuel cell into aerobic granular sludge bioreactor for ciprofloxacin stress alleviation: performance and mechanism, J. Clean. Prod. 373 (2022).

[3] M. Zhang, F. Han, Y. Li, Z. Liu, H. Chen, Z. Li, Q. Li, W. Zhou, Nitrogen recovery by a halophilic ammonium-assimilating microbiome: a new strategy for saline wastewater treatment, Water Res 207 (2021) 117832.

[4] M. Pronk, J. Bassin, M. De Kreuk, R. Kleerebezem, M. Van Loosdrecht, Evaluating the main and side effects of high salinity on aerobic granular sludge, Appl. Microbiol. Biotechnol. 98 (2014) 1339–1348.

[5] S. Okabe, A. Kamizono, S. Kawasaki, K. Kobayashi, M. Oshiki, Interspecific competition and adaptation of anammox bacteria at different salinities: Experimental validation of the Monod growth model with salinity inhibition, Water Res 271 (2025) 122883.

[6] M. Zhang, F. Han, H. Chen, J. Yao, Q. Li, Z. Li, W. Zhou, The effect of salinity on ammonium-assimilating biosystems in hypersaline wastewater treatment, Sci. Total Environ. 829 (2022) 154622.

[7] F. Han, M. Zhang, Z. Li, Z. Liu, Y. Han, Y. Li, W. Zhou, Self-assembly of ammonium assimilation microbiomes regulated by COD/N ratio, Chem. Eng. J. 455 (2023).

[8] C. Zhao, T. Jiao, W. Zhang, Y. Guo, F. Han, J. Lei, W. Zhou, Carbon sources influence on heterotrophic ammonia assimilation: Performance and mechanism, Chem. Eng. J. (497 () (2024).

[9] J. Hou, L. Xia, T. Ma, Y. Zhang, Y. Zhou, X. He, Achieving short-cut nitrification and denitrification in modified intermittently aerated constructed wetland, Bioresour. Technol. 232 (2017) 10–17.

[10] V. Singh, B. Ormeci, S. Mishra, A. Hussain, Simultaneous partial nitrification, ANAMMOX and denitrification (SNAD) – a review of critical operating parameters and reactor configurations, Chem. Eng. J. 433 (2022).

[11] M. Chang, B. Liang, K. Zhang, Y. Wang, D. Jin, Q. Zhang, L. Hao, T. Zhu, Simultaneous shortcut nitrification and denitrification in a hybrid membrane aerated biofilms reactor (H-MBfR) for nitrogen removal from low COD/N wastewater, Water Res 211 (2022) 118027.

[12] C. Zhao, J. Lei, F. Han, T. Jiao, Y. Han, W. Zhou, Novel strategy for treating high salinity oilfield produced water: pyrite-activated peroxymonosulfate coupled with heterotrophic ammonia assimilation, Water Res. (247 () (2023).

[13] C. Zhao, D. Wei, D. Fan, S. Meng, S. Bian, X. Zhang, B. Du, Q. Wei, Coupling of nitrifying granular sludge into microbial fuel cell system for wastewater treatment: System performance, electricity production and microbial community shift, Bioresour. Technol. 326 (2021) 124741.

[14] H. Yuan, Z. Dang, C. Li, Y. Zhou, B. Yang, S. Huang, Simultaneous oxygen and nitrate respiration for nitrogen removal driven by aeration: carbon/nitrogen metabolism and metagenome-based microbial ecology, J. Water Process Eng. 50 (2022).

[15] Z. Wang, Z. Chen, L. Zhu, B. Liu, S. Liu, H. Huang, Q. Wen, Effects of salinity regulation strategies on the enrichment of polyhydroxyalkanoate (PHA) producing mixed cultures: microbial community succession and metabolic mechanisms, Chem. Eng. J. 506 (2025).

[16] H. Tsukamoto, H.V. Phan, T. Suenaga, S. Yasuda, M. Kuroiwa, S. Riya, A. Ogata, T. Hori, A. Terada, Microaerophilic Activated Sludge System for Ammonia Retention toward Recovery from High-Strength Nitrogenous Wastewater: Performance and Microbial Communities, Environ. Sci. Technol. 57 (2023) 13874–13886.

[17] G. Liu, X. Wu, D. Li, L. Jiang, J. Huang, L. Zhuang, Long-term low dissolved oxygen operation decreases N(2)O emissions in the activated sludge process, Environ. Sci. Technol. 55 (2021) 6975–6983.

[18] Z. Qin, X. Ke, C. Wei, H. Zhang, Z. Pang, A. Chen, C. Wei, P. Luo, G. Qiu, Energy-saving mechanism of wastewater treatment process adaptation on natural temperature variation: the case from coking wastewater, Environ. Sci. Technol. 58 (2024) 16399–16409.

[19] E. van Voorthuizen, A. Zwijnenburg, W. van der Meer, H. Temmink, Biological black water treatment combined with membrane separation, Water Res 42 (2008) 4334–4340.

[20] APHA, 2017. Standard Methods for Examination of Water and Wastewater, 23rd Ed. American Public Health Association, Washington.

[21] C. Zhao, T. Jiao, W. Zhang, W. Zhang, M. Jia, S. Liu, M. Zhang, F. Han, Y. Han, J. Lei, X. Wang, W. Zhou, Nutrients recovery by coupled bioreactor of heterotrophic ammonia assimilation and microbial fuel cell in saline wastewater, Sci. Total Environ. 918 (2024) 170697.

[22] C. Zhao, J. Lei, F. Han, T. Jiao, Y. Han, W. Zhou, Novel strategy for treating high salinity oilfield produced water: Pyrite-activated peroxymonosulfate coupled with heterotrophic ammonia assimilation, Water Res 247 (2023) 120772.

[23] W. Zhang, C. Zhao, F. Han, W. Zhang, W. Zhou, Augmented carbon utilization and ammonia assimilation in heterotrophic microorganism under magnetic field stimulation, Environ. Res 269 (2025) 120926.

[24] W. Zhou, J. Hao, Y. Guo, C. Zhao, M. Zhang, S. Zhang, F. Han, Revealing bioresponses of biofilm and flocs to salinity gradient in halophilic biofilm reactor, Bioresour. Technol. 401 (2024).

[25] K.D. Kits, C.J. Sedlacek, E.V. Lebedeva, P. Han, A. Bulaev, P. Pjevac, A. Daebeler, S. Romano, M. Albertsen, L.Y. Stein, H. Daims, M. Wagner, Kinetic analysis of a complete nitrifier reveals an oligotrophic lifestyle, Nature 549 (2017) 269–272.

[26] R. Manser, W. Gujer, H. Siegrist, Membrane bioreactor versus conventional activated sludge system: population dynamics of nitrifiers, Water Sci. Technol. 52 (2005) 417–425.

[27] H.J. Laanbroek, S. Gerards, Competition for limiting amounts of oxygen between Nitrosomonas europaea and nitrobacter winogradskyi grown in mixed continuous cultures, Arch. Microbiol. 159 (1993) 453–459.

[28] B. Nowka, H. Daims, E. Spieck, Comparison of oxidation kinetics of nitrite-oxidizing bacteria: nitrite availability as a key factor in niche differentiation, Appl. Environ. Microbiol. 81 (2015) 745–753.

[29] H.D. Park, D. Noguera, Characterization of two ammonia-oxidizing bacteria isolated from reactors operated with low dissolved oxygen concentrations, J. Appl. Microbiol. 102 (2007) 1401–1417.

[30] R. Blackburne, V.M. Vadivelu, Z. Yuan, J. Keller, Kinetic characterisation of an enriched Nitrospira culture with comparison to Nitrobacter, Water Res. 41 (2007) 3033–3042.

[31] R. Manser, W. Gujer, H. Siegrist, Consequences of mass transfer effects on the kinetics of nitrifiers, Water Res. 39 (2005) 4633–4642.

[32] M.-R. Park, H. Park, K. Chandran, Molecular and kinetic characterization of planktonic Nitrospira spp. selectively enriched from activated sludge, Environ. Sci. Technol. 51 (2017) 2720–2728.

[33] C.E. Lawson, S. Lücker, Complete ammonia oxidation: an important control on nitrification in engineered ecosystems? Curr. Opin. Biotechnol. 50 (2018) 158–165.

[34] M.G. Langille, J. Zaneveld, J.G. Caporaso, D. McDonald, D. Knights, J.A. Reyes, J. C. Clemente, D.E. Burkepile, R.L. Vega Thurber, R. Knight, R.G. Beiko, C. Huttenhower, Predictive functional profiling of microbial communities using 16S rRNA marker gene sequences, Nat. Biotechnol. 31 (2013) 814–821.

[35] H. Yuan, J. Yuan, Y. You, B. Zhang, Y. Wu, S. Huang, Y. Zhang, Simultaneous ammonium and sulfate biotransformation driven by aeration: nitrogen/sulfur metabolism and metagenome-based microbial ecology, Sci. Total Environ. 794 (2021).

[36] Z. Chen, Y. Zhou, Z. Huang, C. Su, X. Wan, Y. Xu, M. Lu, X. Lin, Effects of sulfate concentration and external voltage on operation efficiency, sludge characteristics, and microbial community of a bioelectrochemical system, Biochem. Eng. J. 198 (2023).

[37] C. Jiang, Z. Zhao, D. Zhu, X. Pan, Y. Yang, Rare resistome rather than core resistome exhibited higher diversity and risk along the Yangtze River, Water Res 249 (2024) 120911.

[38] P. Ouyang, H. Wang, I. Hajnal, Q. Wu, Y. Guo, G.Q. Chen, Increasing oxygen availability for improving poly(3-hydroxybutyrate) production by Halomonas, Metab. Eng. 45 (2018) 20–31.

[39] G. Guo, X. Li, F. Tian, T. Liu, F. Yang, K. Ding, C. Liu, J. Chen, C. Wang, Azo dye decolorization by a halotolerant consortium under microaerophilic conditions, Chemosphere 244 (2020) 125510.

[40] N. Nazari, F.Jookar Kashi, A novel microbial synthesis of silver nanoparticles: Its bioactivity, Ag/Ca-Alg beads as an effective catalyst for decolorization Disperse Blue 183 from textile industry effluent, Sep. Purif. Technol. 259 (2021).

[41] G. Gahlawat, A.K. Srivastava, Development of a mathematical model for the growth associated Polyhydroxybutyrate fermentation by Azohydromonas australica and its use for the design of fed-batch cultivation strategies, Bioresour. Technol. 137 (2013) 98–105.

[42] W.A. Alsiary, M.M.Y. Madany, H. AbdElgawad, The pleiotropic role of Salinicoccus bacteria in enhancing ROS homeostasis and detoxification metabolism in soybean and oat to cope with pollution of triclosan, Plant Physiol. Biochem 207 (2024) 108327.

[43] T. He, J. Bao, Y. Leng, S. Kong, J. Du, X. Li, Rice straw particles covered with Brevundimonas naejangsanensis DD1 cells can synergistically remove doxycycline from water using adsorption and biotransformation, Chemosphere 291 (2022) 132828.

[44] J. Chen, B. Zhang, X. Yang, Y. Liu, Z. Zhang, W. Huang, Z. Zhao, Feasibility of ferrous iron addition to promote the pure Chlorella sp. granulation for mariculture wastewater treatment, Bioresour. Technol. Rep. 30 (2025).

[45] Z. Ma, L. Lin, J. Xi, X. Gong, J. Wang, P. Peng, Y. An, W. Hu, J. Cao, Z. Wu, Z. Zhou, Nitrogen removal from dewatering liquid of landfill sludge by partial nitrification and denitrification, Bioresour. Technol. 390 (2023) 129856.

[46] M.R. Kelly, P. Whitworth, A. Jamieson, J.G. Burgess, Bacterial colonisation of plastic in the Rockall Trough, North-East Atlantic: An improved understanding of the deep-sea plastisphere, Environ. Pollut. 305 (2022) 119314.

[47] J. Chen, M. Gao, Y. Zhao, L. Guo, C. Jin, J. Ji, Z. She, Nitrogen and sulfamethoxazole removal in a partially saturated vertical flow constructed wetland treating synthetic mariculture wastewater, Bioresour. Technol. 358 (2022) 127401.

[48] Q. Li, Y. Wang, C. An, H. Jia, J. Wang, Exploring novel approaches to enhance start-up process in microbial fuel cell: A comprehensive review, J. Water Process Eng. 63 (2024).

[49] X. Cai, Y. Hu, S. Zhou, D. Meng, S. Xia, H. Wang, Unraveling bacterial and eukaryotic communities in secondary water supply systems: Dynamics, assembly, and health implications, Water Res. 245 (2023) 120597.

[50] J. Chave, Neutral theory and community ecology, Ecol. Lett. 7 (2004) 241–253.

[51] Z. Qiao, R. Sun, Y. Wu, S. Hu, X. Liu, J. Chan, X. Mi, Characteristics and metabolic pathway of the bacteria for heterotrophic nitrification and aerobic denitrification in aquatic ecosystems, Environ. Res 191 (2020) 110069.
[52] P. Kundu, A. Pramanik, A. Dasgupta, S. Mukherjee, J. Mukherjee, Simultaneous heterotrophic nitrification and aerobic denitrification by Chryseobacterium sp. R31 isolated from abattoir wastewater, Biomed. Res Int 2014 (2014) 436056.
[53] P. Kundu, A. Pramanik, S. Mitra, J.D. Choudhury, J. Mukherjee, S. Mukherjee, Heterotrophic nitrification by Achromobacter xylosoxidans S18 isolated from a small-scale slaughterhouse wastewater, Bioprocess Biosyst. Eng. 35 (2012) 721–728.
[54] M. Redmile-Gordon, A.S. Gregory, R.P. White, C.W. Watts, Soil organic carbon, extracellular polymeric substances (EPS), and soil structural stability as affected by previous and current land-use, Geoderma 363 (2020) 114143.